

Oxidation resistance and microstructure of the oxide layers for TiB₂-based cermets

M. G. Barandika,^{a*}† J. J. Echeberría,^b J. M. Sánchez^b and F. Castro^b

^aDpto. Química Inorgánica, Fac. de Farmacia, UPV-EHU. Apdo 450 Vitoria E-01080, Spain

^bDpto. Materiales, CEIT. Apdo 1555 San Sebastián E-20009, Spain

The oxidation behaviour of several TiB₂ cermets has been studied in air in a range of temperatures between 700 and 1000 °C for up to 70 h. The oxidation resistance of these materials has been characterised through measurements of mass gain as a function of time and temperature. The oxidation kinetics of these cermets was observed to change from a parabolic to a linear type at temperatures between 750 and 775 °C. Activation energies were observed to be 170–185 and 109–123 kJ mol⁻¹ for the parabolic and linear ranges, respectively. The oxidation products and the microstructure of the oxide scales formed after these oxidation treatments were characterised by XRD and SEM.

Introduction

As reported before,^{1,2} TiB₂ has been used as a base material for the development of a new family of hard and tough cemented borides for application as cutting and mining tools, wire and tube drawing dies and wear components. These cemented borides are constituted by a major hard dispersed phase (TiB₂) bonded by minor amounts of (Fe–Ni–Al)-based metallic alloys. Sintering of these materials to full density was carried out by several routes and the details are reported elsewhere.^{1,3} The mechanical properties of these cermets, particularly hardness and toughness, are very similar to those found among the best grades of WC–Co hard metals, with the additional advantage of being much lighter (theoretical density ≈ 5.2 g cm⁻³).

Since these cermets have been recently developed, several of their properties are still under current research.⁴ The present paper reports on their oxidation resistance at temperatures between 700 and 1000 °C. The results of this research work will be compared to those reported in the literature^{5–8} for TiB₂ ceramics which constitute the only data available on oxidation for this type of boride.

Additionally, as reported for other ceramic materials,^{9–13} the microstructure and chemical composition of the oxide layer vary with depth from its surface to the vicinity of the substrate as a function of the time and the temperature of the oxidation treatment. Consequently, a full microstructural characterisation of the oxide scales obtained after oxidation of these cermets is also included in this work.

Experimental procedure

Powder mixtures shown in Table 1 were prepared in a turbula mixer during 6 h. Green compacts 16 mm in diameter and 5 mm in height were obtained by uniaxial pressing to blended powders and subsequently sintered to full density at 1500 °C and 100 MPa using a holding period of 1 h. After sintering, the specimens were mechanically ground and polished to 1 μm finish and weighed to an accuracy of 10⁻⁴ g. The oxidation experiments were performed in the temperature range between 700 and 1000 °C for up to 70 h in air. In order to record the mass gains during the oxidation treatments, the specimens were withdrawn from the furnace at fixed time intervals. After oxidation, the mass gained by each specimen was measured several times and the result expressed as an average. These

Table 1 Chemical composition (wt%) of the experimental cermets subjected to the oxidation treatment

cermet	TiB ₂	Fe	Ni	Ti	Al
S20	71.60	14.30	6.10	2.96	5.04
S30	64.30	18.00	7.70	3.70	6.30

specimens were also used for XRD microstructural characterisation. Areas under some selected peaks for each phase were used to qualitatively compare the changes in concentration on the surface of the oxide scale according to expression (1).

$$P_i = \frac{A_i}{\sum A_i} \times 100 \quad (1)$$

where A_i is the area under the following peaks: {101} for TiO₂, {112} for Fe₂Ti₂O₇ and {230} for Fe₃Ti₃O₁₀; $\sum A_i$ is the sum of the areas under the aforementioned peaks, and P_i is the relative peak area for the aforementioned specimens.

Although P_i values do not represent any real concentrations, they can be used to graphically describe the tendencies corresponding to the changes of concentration on the surface of the oxide scale which have been also observed by SEM analysis as the scale gets thicker.

At the end of the oxidation treatments, a selection of specimens were used for SEM in order to characterise the microstructure of the oxide scales (Fig. 1) following a procedure reported elsewhere.^{10,11}

Results

The oxidation behaviour of TiB₂ cermets, whose chemical compositions are summarised in Table 1, was characterised in terms of their oxidation kinetics through measurements of their mass change per surface area ($\Delta m/s$) at various temperatures and times. These results are reported in Fig. 2 and 3. In both cases a change in the oxidation kinetics is observed as a function of temperature, being of a parabolic type at temperatures up to 750 °C and of a linear type at temperatures above 775 °C. Expressions (2) [for the parabolic range ($t \leq 750$ °C)] and (3) [for the linear range ($t \geq 775$ °C)] represent the corresponding mathematical equations for the oxidation kinetics of

†E-mail: qipbaarg@lg.ehu.es

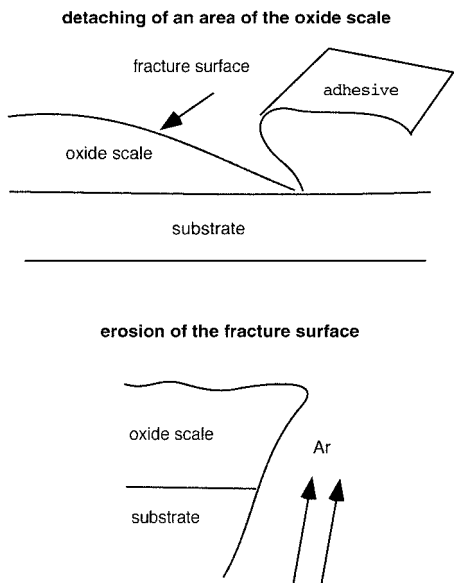


Fig. 1 Schematic representation of the procedure followed for the preparation of SEM samples. (Top) Detaching of an area of the oxide scale using an adhesive and (bottom) the subsequent erosion of the resulting fracture surface by argon ions.

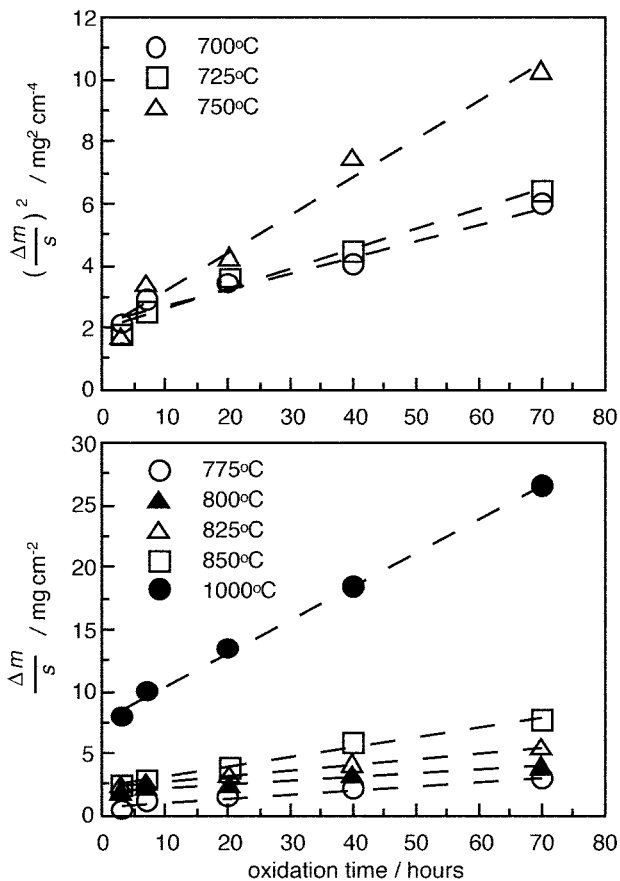


Fig. 2 Oxidation kinetics for specimen S20 indicating (top) a parabolic type and (bottom) a linear type of kinetics for temperature ranges of 700–750 and 775–1000 °C, respectively

these materials.

$$\left(\frac{\Delta m}{s}\right)^2 = A_p + K_p t \quad (2)$$

$$\frac{\Delta m}{s} = A_l + K_l t \quad (3)$$

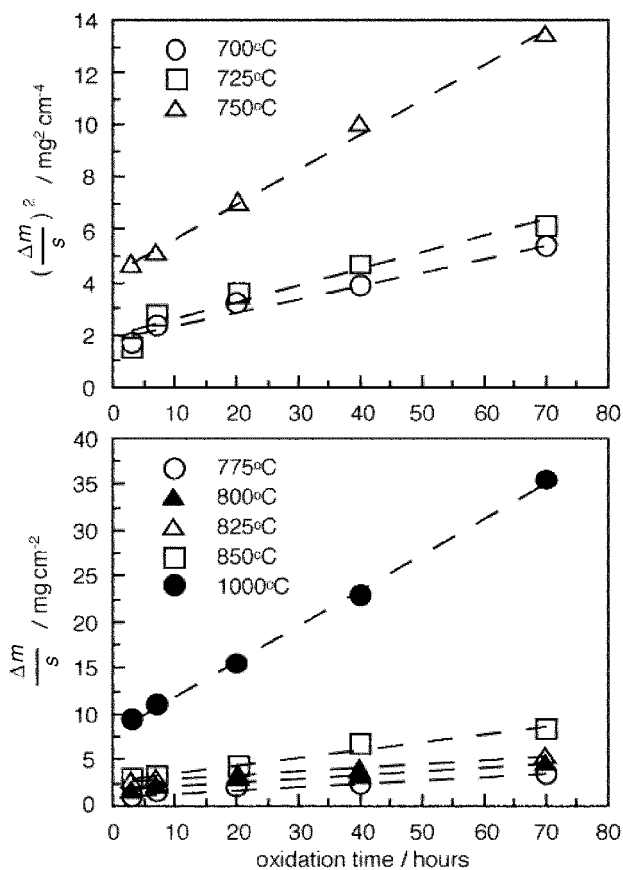


Fig. 3 Oxidation kinetics for specimen S30 indicating (top) a parabolic type and (bottom) a linear type of kinetics for temperature ranges of 700–750 and 775–1000 °C, respectively

where t is the oxidation time and A_p , K_p , A_l and K_l represent the oxidation kinetics constants, whose values for all the experimental oxidation temperatures and compositions are summarised in Table 2.

On these bases, considering the Arrhenius type of plots (Fig. 4) for each range, the values of the corresponding activation energies for each composition are reported in Table 3. As observed in Table 3, the activation energies, Q , turned out to be very similar for both cermets, their values being between 170 and 185 kJ mol⁻¹ for the parabolic range and 109–123 kJ mol⁻¹ for the linear range.

XRD and SEM microstructural characterisation of the oxide scales showed that several oxides were present: rutile-type TiO₂, Nd₂³⁺Ti₂⁴⁺O₇-type Fe₂Ti₂O₇, Fe₂³⁺Mg²⁺Ti₃⁴⁺O₁₀

Table 2 Kinetic constants for oxidation of the experimental materials [A_p (kg² m⁻⁴), A_l (kg m⁻²), K_p (kg² m⁻⁴ s⁻¹) and K_l (kg m⁻² s⁻¹)]

parabolic range	S20		S30		
	$K_p \times 10^8$	$A_p \times 10^4$	$K_p \times 10^8$	$A_p \times 10^4$	
700 °C	1.012	2.71	1.276	236	
725 °C	1.526	2.31	1.710	219	
750 °C	2.802	3.58	3.892	455	
linear range	S20		S30		
	$K_l \times 10^7$	$A_l \times 10^2$	$K_l \times 10^7$	$A_l \times 10^2$	
	775 °C	0.862	7.8	0.945	9.2
	800 °C	1.001	14.4	1.084	15.1
	825 °C	1.557	15.4	1.501	13.2
	850 °C	2.252	19.8	2.280	22.1
1000 °C	7.506	75.2	10.564	79.7	

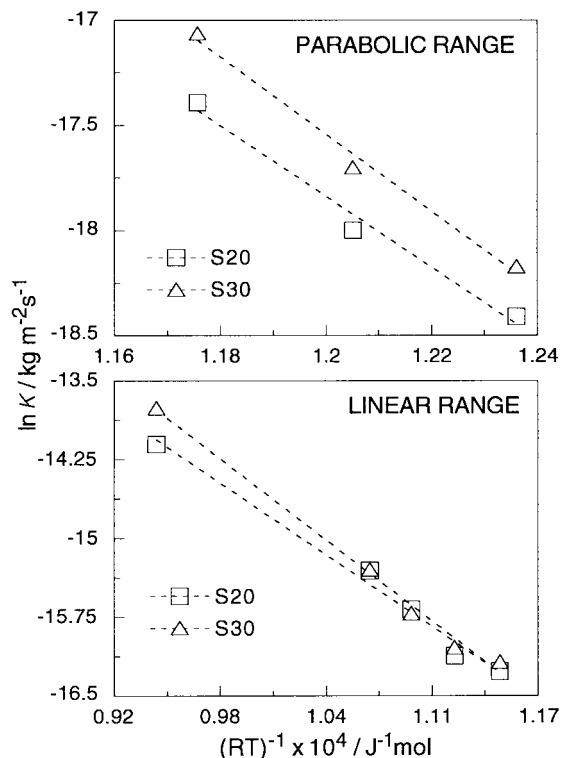


Fig. 4 Arrhenius plots for specimens S20 and S30 corresponding to the parabolic range and the linear range of oxidation kinetics

Table 3 Oxidation kinetics constants obtained from Arrhenius plots for both experimental materials, [$K = K_o \exp(-Q/RT)$]

parabolic range			linear range	
$K_o / \text{kg}^2 \text{m}^{-4} \text{s}^{-1}$	$Q / \text{kJ mol}^{-1}$	cermet	$K_o \times 10^2 / \text{kg m}^{-2} \text{s}^{-1}$	$Q / \text{kJ mol}^{-1}$
12.47	170	S20	23.69	109
97.03	185	S30	121.27	123

(kennedyite)-type $\text{Fe}_3\text{Ti}_3\text{O}_{10}$ and $\text{Fe}_2\text{NiTi}_3\text{O}_{10}$. These oxides have been identified by TEM in similar oxidised specimens.¹⁴ Some Al-oxides have also been observed which, according to SEM analysis and on the basis of the aforementioned TEM¹⁴ characterisation, are corundum-type Al_2O_3 . Complex oxides $\text{Fe}_2\text{Ti}_2\text{O}_7$, $\text{Fe}_3\text{Ti}_3\text{O}_{10}$ and $\text{Fe}_2\text{NiTi}_3\text{O}_{10}$ contain small amounts of Al (<2 atom%). Additionally, in $\text{Fe}_3\text{Ti}_3\text{O}_{10}$ oxides, nickel can be found in low proportions (<6 atom%). In contrast, no Ni has been found in $\text{Fe}_2\text{Ti}_2\text{O}_7$ oxides. TiO_2 (in both ranges) and complex oxides $\text{Fe}_2\text{Ti}_2\text{O}_7$ (in the parabolic range) and $\text{Fe}_3\text{Ti}_3\text{O}_{10}$ (in the linear range) are the major phases on the surface of the oxide scales of the oxidised specimens. Complex oxides $\text{Fe}_2\text{NiTi}_3\text{O}_{10}$ have only been found in specimens oxidised in the parabolic range in very low proportions (2 vol%). In Fig. 5, several XRD traces are shown in which progression in time and temperature of the composition of the oxide scale for specimen S30 can be seen.

Fig. 6 represents a summary of the information gathered through XRD after various oxidation times for specimens cut from material S30. This information is also representative for the material S20. It can be seen that the relative peak area of TiO_2 on the surface of the oxide scale continuously decreases with oxidation time (*i.e.* with the thickness of the scale) at temperatures corresponding to both ranges, while relative peak areas of $\text{Fe}_2\text{Ti}_2\text{O}_7$, in the parabolic range, and $\text{Fe}_3\text{Ti}_3\text{O}_{10}$, in the linear range, increase.

As reported before,⁹⁻¹² the oxidation behaviour of multiphase materials is closely related to the microstructural

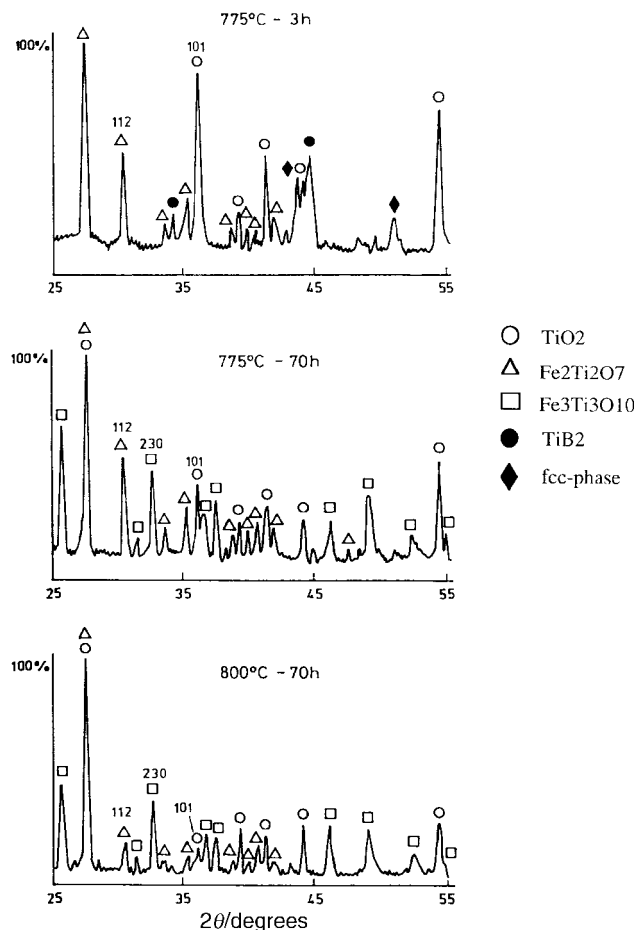


Fig. 5 XRD traces corresponding to the surface of the oxide scale for S30 specimens after the following oxidation treatments: 3 h at 775 °C, 70 h at 775 °C and 70 h at 800 °C

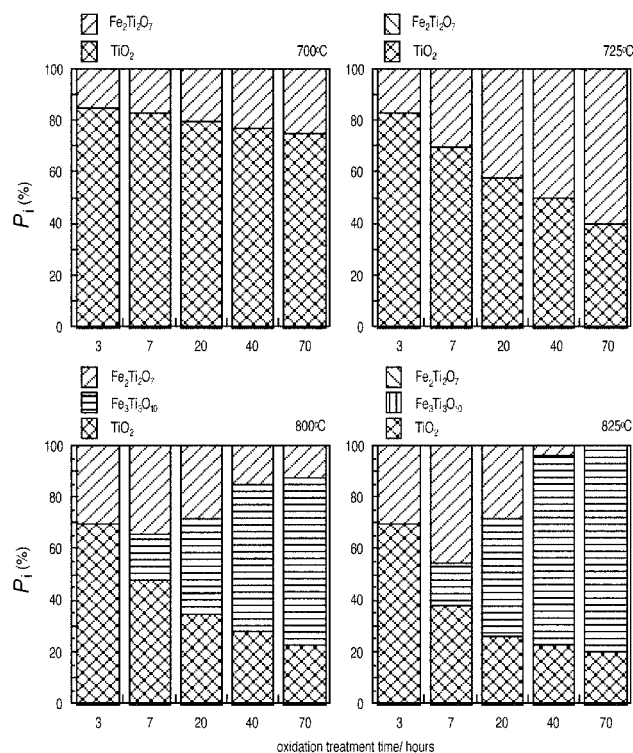


Fig. 6 Progression in time of the relative areas of the XRD peaks {101}- TiO_2 , {112}- $\text{Fe}_2\text{Ti}_2\text{O}_7$ and {230}- $\text{Fe}_3\text{Ti}_3\text{O}_{10}$ on the surface of the oxide scales corresponding to S30 specimens oxidised at different temperatures

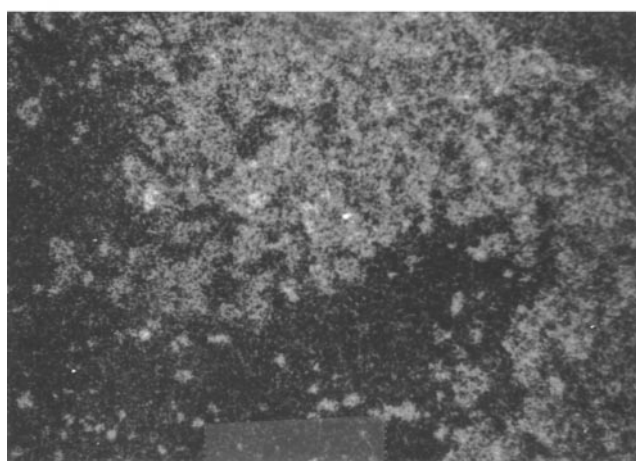
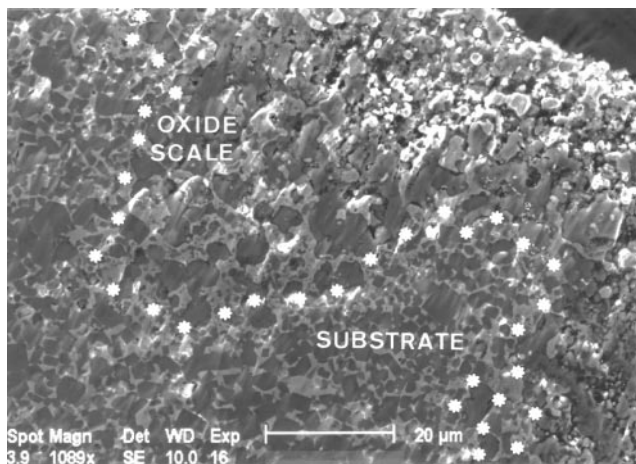


Fig. 7 (Top) Micrograph corresponding to a fracture surface of the oxide scale of a S30 specimen after 70 h oxidation treatment at 850 °C and (bottom) a X-ray mapping of the same fracture surface illustrating the distribution of oxygen (white) and boron (dark)

development of the oxide scale. In materials S20 and S30 the microstructure of the oxide scales has also been observed to vary in depth from their surface to the vicinity of the substrate. This is illustrated in Fig. 7 for specimen S30 after 70 h oxidation treatment. In the same figure, an X-ray mapping of boron and oxygen clearly reveals the limits between the substrate and the oxide scale. A careful analysis of all the oxidised specimens corresponding to both cermets (S20 and S30) showed that the oxide scales exhibit at least four distinguishable sublayers (micrographs in Fig. 8 and 9). These micrographs are representative for the specimens oxidised at temperatures corresponding to the parabolic (Fig. 8) and linear range (Fig. 9). In relation to the phases present in each sublayer, it must be pointed out that, since TiO₂ and the Fe,Ti complex oxides form a continuous bumpy matrix, the differentiation between these phases by their morphology is rather difficult. Then, the identification of the phases (described below) has been done by combining XRD and EDS information.

Parabolic range

Fig. 8A—first sublayer. A substrate area can be seen in which grey grains of TiB₂ are surrounded by the metallic Fe,Ni,Al binder phase. An area corresponding to the first oxide sublayer can also be seen in which TiO₂ is the major constituent (grey contrast). The white grains correspond to Fe and Ni oxides while the black ones are Al₂O₃.

Fig. 8B—second sublayer. TiO₂ is also the major constituent but Fe,Ti complex oxides (lighter contrast) can also be

distinguished. White and dark grains correspond to Ni oxides and Al₂O₃, respectively.

Fig. 8C—third sublayer. Three types of oxides can be seen: TiO₂ (grey), Al₂O₃ (dark) and, Fe,Ti complex oxides (light).

Fig. 8D—fourth sublayer. Larger grains of TiO₂ (grey), and Fe,Ti complex oxides (lighter) can be distinguished.

Linear range

Fig. 9A—first sublayer. Grains of TiO₂ (3–9 μm) can be seen surrounded by a continuous (Fe,Ni)₂B phase containing no oxygen at all. Black grains are Al₂O₃.

Fig. 9B—second sublayer. Grains of TiO₂ (grey) and Fe,Ti complex oxides (lighter) can be observed. Dark areas correspond to Al₂O₃.

Fig. 9C—third sublayer. Most of the grains correspond to Fe,Ti complex oxides while the proportion of TiO₂ is lower.

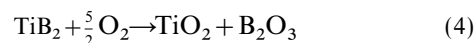
Fig. 9D—fourth sublayer. Grains of Fe,Ti complex oxides are forming a continuous scale. A very low proportion of TiO₂ (grey) is present.

The gradient of the complex oxides Fe₂Ti₂O₇ and Fe₃Ti₃O₁₀ was confirmed by SEM to follow the profiles described in Fig. 6 for both temperature ranges. It is also worth mentioning that Fe:Ti atomic ratios determined by SEM analysis on the surface of the oxide scales of specimens oxidised at different temperatures corresponding to the parabolic range are very similar to the values in the substrate (*ca.* 1:6 and *ca.* 1:4 for S20 and S30, respectively). On the surface of the oxide scales of the specimens oxidised at different temperatures corresponding to the linear range, in contrast, SEM analysis revealed that Fe:Ti atomic ratios tend to 1:1 for increasing temperatures and times.

Discussion

Considering the type of oxidation kinetics for TiB₂ ceramics^{5–8} which is parabolic below 900 °C, cubic between 900 and 950 °C and parabolic again above 950 °C, it may be realised that TiB₂ cermets exhibit worse oxidation resistance than TiB₂ ceramics. This behaviour must be related to the existence of a metallic binder phase in TiB₂ cermets as described below.

In general, it may be understood that TiO₂ is the main oxidation product formed. The formation of TiO₂ in both temperature ranges (parabolic and linear) is due to the oxidation of TiB₂ through the following reaction:



Since no crystalline B₂O₃ has been found by XRD analysis of the oxides scales, the following has been considered. Boric oxide B₂O₃ could be present as a glassy phase which is not detected by EDS analysis. The crystalline material melts at 450 °C whereas the glassy one softens over a wide temperature range. Although the boiling point lies above 1500 °C, liquid B₂O₃ exhibits noticeable volatility.¹³ Therefore, a fraction of B₂O₃ could have disappeared from the oxide scales during the oxidation treatments.

The formation of Al₂O₃ is clearly understood in terms of the oxidation of aluminium from the binder phase. Additionally, aluminium and nickel must be expected to be partially occupying the M³⁺ and M²⁺ sites in the complex oxides (as Al³⁺ and Ni²⁺). No nickel has been found in Fe₂Ti₂O₇ as this oxide does not have any sites for M²⁺ cations. Therefore, Ni oxides which were found in the first and second sublayers (Fig. 8A and B) are thought to be NiO.

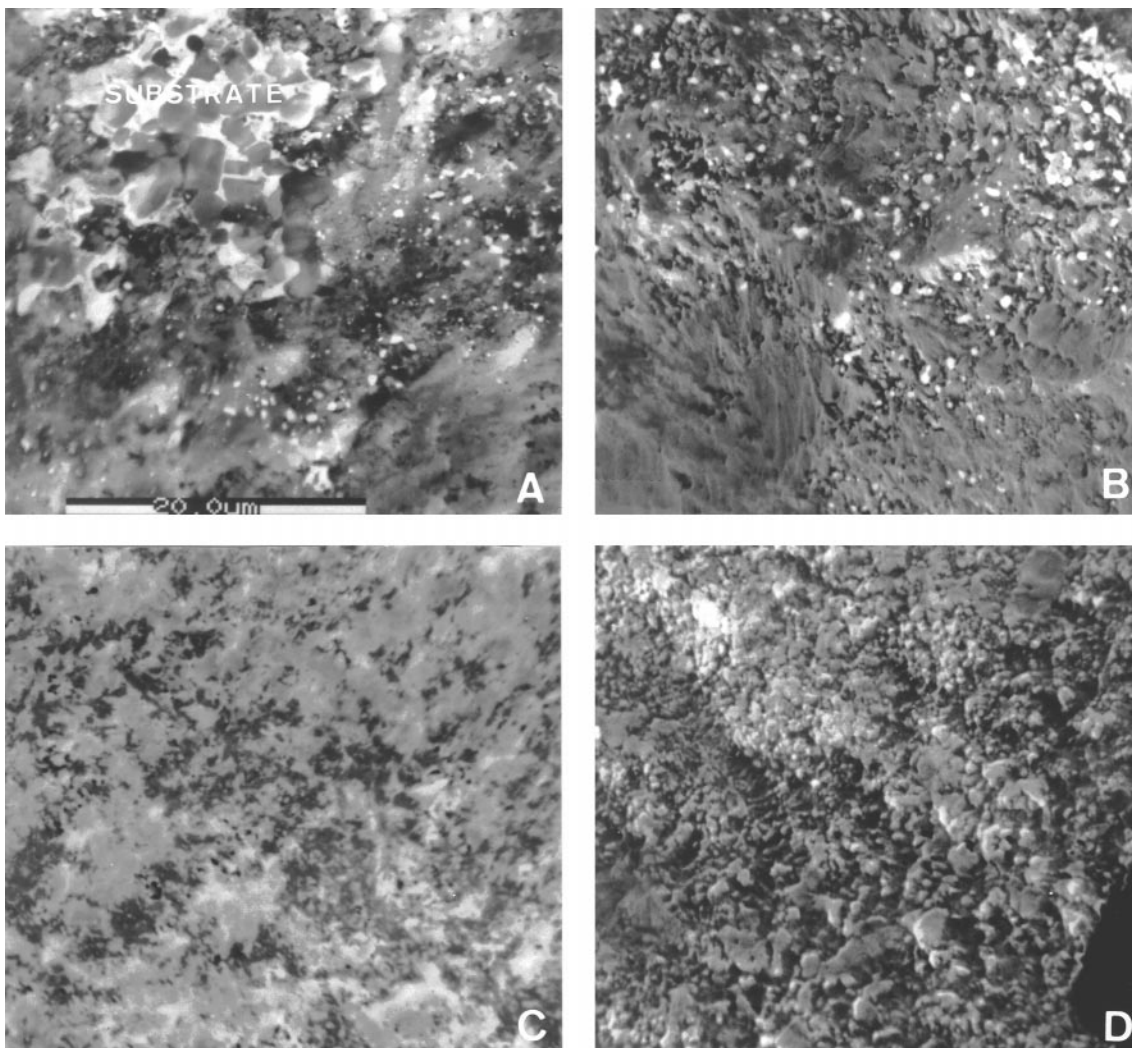


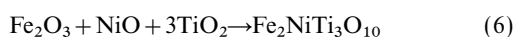
Fig. 8 Micrographs corresponding to the oxide sublayers for specimen S20 after 70 h oxidation treatment at 700 °C. The sequence of the micrographs goes from (A) the vicinity of the substrate to (D) the surface of the oxide scale. The magnification is the same for the four micrographs.

In order to explain the formation of the complex oxides $\text{Fe}_2\text{Ti}_2\text{O}_7$, the following reaction is proposed:



Progression of reaction (5) in time could explain the decrease of TiO_2 and the increase of $\text{Fe}_2\text{Ti}_2\text{O}_7$ on the surface of the oxide scale in specimens oxidised in the parabolic range (Fig. 6). Differences in relative peak areas for TiO_2 and $\text{Fe}_2\text{Ti}_2\text{O}_7$ corresponding to different temperatures cannot be directly interpreted due to the increasing thickness of the oxide scales for increasing temperatures.

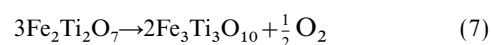
In specimens oxidised in the parabolic range, a low amount of $\text{Fe}_2\text{NiTi}_3\text{O}_{10}$ has also been observed whose formation can be described as follows:



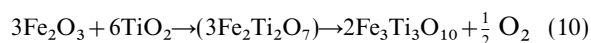
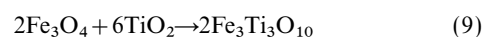
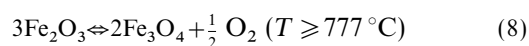
Obviously, Fe_2O_3 should be the product of the oxidation of iron which is the major constituent of the metallic binder phase. This oxide has not been identified by XRD, as it is supposed to form and immediately disappear to form the complex oxides. Only in the vicinity of the substrate (Fig. 9A), some of the small white grains could be thought to be Fe_2O_3 (according to SEM analysis).

In relation to the experimental results corresponding to the linear range, data in Fig. 6 suggest that the formation of $\text{Fe}_3\text{Ti}_3\text{O}_{10}$ takes place, somehow, at the expense of the forma-

tion of $\text{Fe}_2\text{Ti}_2\text{O}_7$, as expressed by reaction (7).



Reaction (7) represents the reduction of a fraction of Fe^{3+} (in $\text{Fe}_2^{3+}\text{Ti}_2^{4+}\text{O}_7$) to Fe^{2+} giving $\text{Fe}_2^{3+}\text{Fe}^{2+}\text{Ti}_3^{4+}\text{O}_{10}$ and liberating oxygen. This reaction could be expressed as a combination of reactions (8) and (9), as follows.



Thus, reaction (7) could be understood as the decomposition of Fe_2O_3 (an equilibrium which according to thermodynamic data^{15,16} takes place at temperatures above 777 °C) and the subsequent formation of $\text{Fe}_3\text{Ti}_3\text{O}_{10}$ by direct reaction of Fe_3O_4 and TiO_2 .

Taking into account the conditions of the oxidation treatments, the occurrence of reaction (7) should be interpreted to take place along with the oxidation of the rest of the specimens, as expressed by reaction (11). Therefore, combination of reactions (7) and (11) results in the redox reaction (12) which could describe the global process corresponding to the linear range.

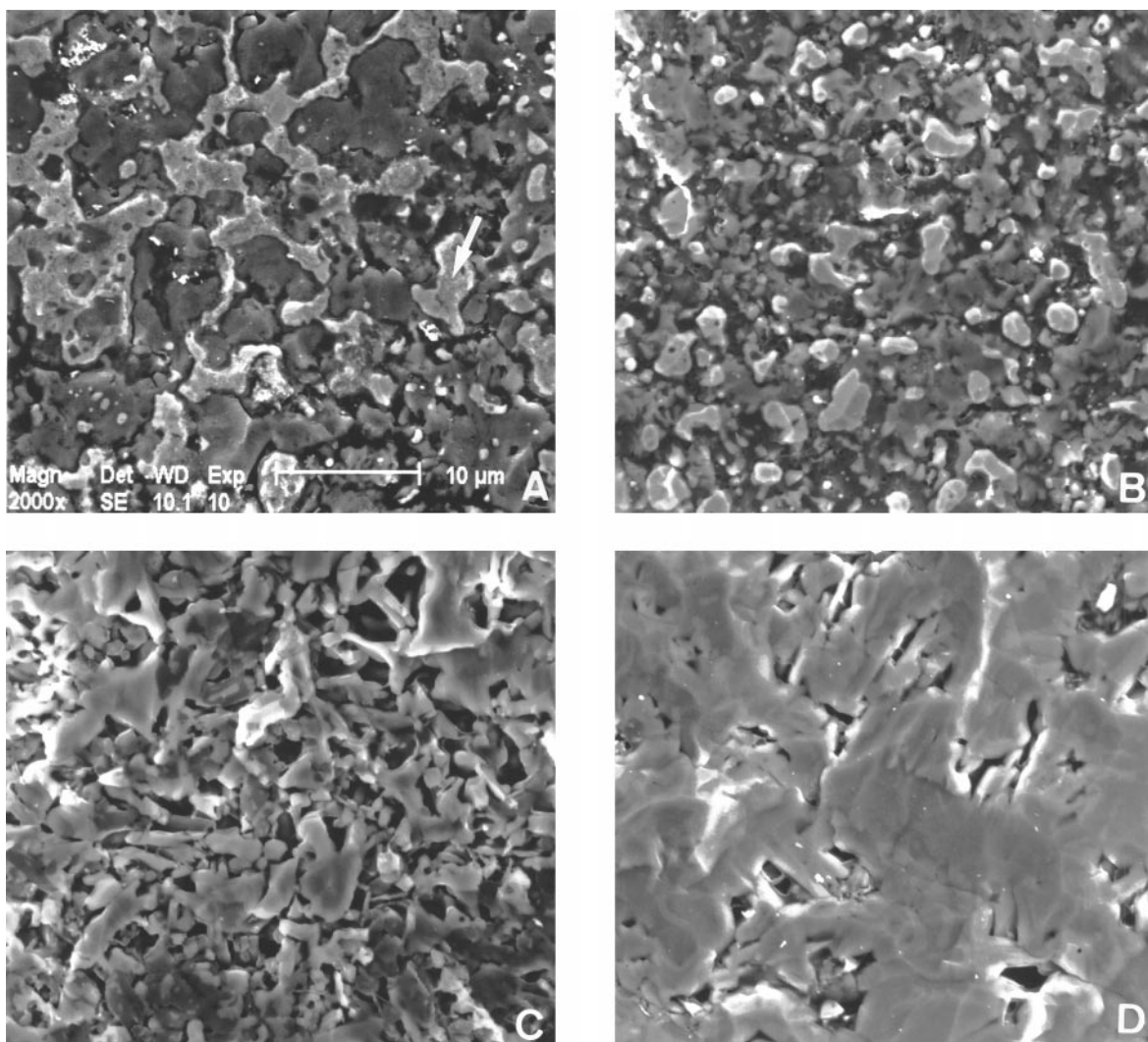
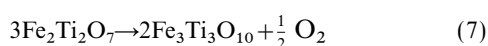


Fig. 9 Micrographs corresponding to the oxide sublayers for specimen S30 after 70 h oxidation treatment at 850 °C. The sequence of the micrographs goes from (A) the vicinity of the substrate to (D) the surface of the oxide scale. The magnification is the same for the four micrographs. An area of the phase $(\text{Fe,Ni})_2\text{B}$ is marked with the arrow.



where A_r represents the specimens in their reduced forms (TiB_2 , Ni, Al) and AO represents the oxidised specimens (TiO_2 , B_2O_3 , Al_2O_3 , NiO).

A scheme of the reactions involved in each kinetic range can be seen in Fig. 10.

Microstructural analysis of the specimens oxidised in the linear range shows that the $\text{Fe}_3\text{Ti}_3\text{O}_{10}/\text{TiO}_2$ volumetric ratio in the surface of the oxide scale at the end of the oxidation treatment is much higher than that expected by considering the relative amounts of iron and titanium in the substrate. In particular, as mentioned before, while in the specimens oxidised in the parabolic range the Fe:Ti atomic ratio keeps constant along the oxide scale, in the specimens oxidised in the linear range this ratio changes from 1:6 and 1:4 (for specimens S20 and S30, respectively) in the substrate to values close to 1:1. This fact can be related to the presence of secondary borides in the vicinity of the substrate of specimens oxidised in the linear range (Fig. 9A) as well as to the reduction of Fe_2O_3 [reaction (8)].

Firstly, as iron is more concentrated in the outer part of the oxide scale, the concentration of the rest of the elements must

be relatively higher in the vicinity of the substrate. Thus, as titanium, boron, aluminium and nickel are more concentrated in relation to iron, greater competition for the oxygen is established in the vicinity of the substrate which results in the fact that there is not as much oxygen as required for iron, nickel and boron to form oxides (aluminium and titanium have higher affinities for oxygen). Therefore, iron and nickel achieve a higher oxidation state by forming $(\text{Fe,Ni})_2\text{B}$ secondary borides. This chemical behaviour has been positively identified in several TiB_2 -Fe and TiB_2 -Fe,Ni cermets in which oxygen is present as an impurity.^{1,17,18}

On the other hand, the condition of equilibrium of reaction (8) could influence the composition of the oxide scale as follows. According to Le Chatelier's law, when at a particular moment and place oxygen vapour has been consumed by reaction (11), the relative amount of $\text{Fe}_2\text{Ti}_2\text{O}_7$ should decompose. Obviously, there is a finite amount of $\text{Fe}_2\text{Ti}_2\text{O}_7$ at that particular moment and place, but also a certain amount of TiO_2 left [*i.e.* which has not taken part in reaction (5)]. Then, Fe_2O_3 [the limiting reactant for reaction (5)] should be provided at this particular moment and place, in order to form the required amount of $\text{Fe}_2\text{Ti}_2\text{O}_7$. This is in accordance with the fact that, in the linear range, a constant oxidation of iron (from Fe^0 in the substrate to Fe^{3+} in the oxide scale) is taking place. This way, as reactions (5) and (7) continuously progress in time, the composition of the surface of the scales tend to

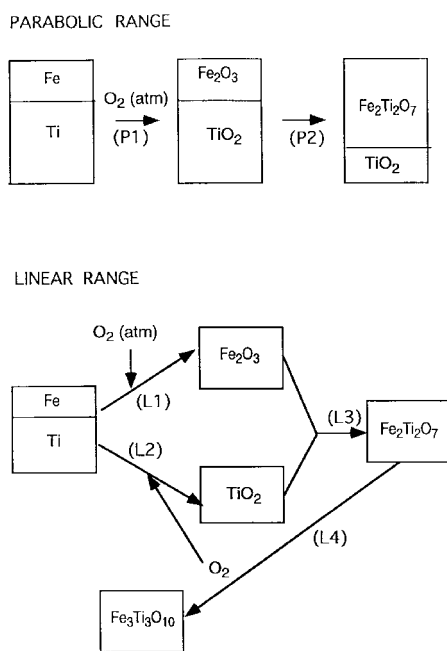


Fig. 10 Simple scheme of the most important reactions taking place in both kinetic ranges. (Top) In the parabolic range, the formation of the TiO_2 and Fe_2O_3 oxides (P1) is followed by the formation of the stoichiometric amount of $\text{Fe}_2\text{Ti}_2\text{O}_7$ (P2). As Fe_2O_3 is the limiting reactant, there is TiO_2 left. (Bottom) In the linear range, the formation of Fe_2O_3 is due to the incorporation of oxygen from the atmosphere (L1) while the formation of TiO_2 (L2) is mainly due to the oxygen liberated by the reduction of $\text{Fe}_2\text{Ti}_2\text{O}_7$ (L4). As this reduction in equilibrium continuously progresses in time, the oxygen gain (due to reaction L1) is constant in time. For this to occur, a constant oxidation of iron is taking place which provides the required amount of Fe_2O_3 to react with TiO_2 giving $\text{Fe}_2\text{Ti}_2\text{O}_7$ (L3).

$\text{Fe}_3\text{Ti}_3\text{O}_{10}$ (in agreement with values of Fe:Ti atomic ratios tending to 1:1).

Since the decomposition of Fe_2O_3 [reaction (8)] takes place at temperatures above 777°C ,^{15,16} this reaction must be related to the change in kinetics from parabolic to linear (which according to experimental results takes place at a temperature between 750 and 775°C). This small disparity between temperatures can be explained by considering that $\text{Fe}_2\text{Ti}_2\text{O}_7$ and $\text{Fe}_3\text{Ti}_3\text{O}_{10}$ oxides contain small amounts of Al (and Ni in $\text{Fe}_3\text{Ti}_3\text{O}_{10}$). Then, the presence of these elements could cause the reduction of Fe_2O_3 to start at a slightly lower temperature.

The change in kinetics from parabolic to linear can be caused by either a change in the mechanism of oxidation or, alternatively, by a second mechanism in the linear range in addition to the one operating in the parabolic range. Even if a discussion of this latest point should be rather tentative, the following argument could be considered. It may be thought that, in the parabolic range, mass gain (*i.e.* oxygen gain) becomes slower as the oxidation goes on because of a slower diffusion of oxygen to the vicinity of the substrate as the distance from the atmosphere is longer. In contrast, at temperatures above 777°C , the gain of oxygen with time is constant. At these temperatures, the rate of incorporation of oxygen from the atmosphere to the scale should be controlled by the necessity of a constant oxidation of Fe in time and its subsequent reduction (Fig. 10). This reduction represents a new

way of transporting oxygen to the substrate which does not take place in the parabolic range. Then, in the linear range of temperatures, the oxygen gain does not depend on the thickness of the scale but on the constant progression in time of the equilibrium of reduction.

Concluding remarks

The oxidation of TiB_2 cermets containing a Fe-rich binder phase in air is observed to present two oxidation ranges, of parabolic type below 750°C and linear type above 775°C .

The two types of oxidation kinetics are accompanied by the formation of oxide scales with different chemical compositions and microstructures. It is common to both oxidation ranges that the oxide scales formed are constituted by at least four distinguishable oxide sublayers having a distinct microstructure from the surface to the vicinity of the substrate.

The microstructural development of the oxides scales can be explained in terms of the formation of Fe,Ti complex oxides in specimens oxidised at temperatures corresponding to both parabolic and linear ranges.

The transition in kinetics from parabolic to linear has been proposed to be related to the reduction in equilibrium of a fraction of Fe^{3+} to Fe^{2+} (at temperatures above 777°C) and the subsequent oxidation of the rest of the specimens.

The authors gratefully acknowledge the financial support of the European Committee through the Brite Project EEC BRITE PROJECT P.2293, Development of new boride-based cermets and ceramics (Contract No. RI 1 B-0219.c), for the realisation of this work.

References

- 1 J. M. Sánchez, M. G. Barandika, J. Gil-Sevillano and F. Castro, *Scripta Metall. Mater.*, 1992, **26**, 957.
- 2 M. G. Barandika, J. M. Sánchez and F. Castro, *Met. Powder Rep.*, 1994, **49**, 10.
- 3 M. G. Barandika, J. M. Sánchez and F. Castro, in *Proceedings of Third Euro-Ceramics V.1*, ed. P. Duran and J. F. Fernández, Faenza Editrice Iberica, Castellón de la Plana, Spain, 1993, pp. 1115–1120.
- 4 R. González, M. G. Barandika, D. Oña, J. M. Sánchez, A. Vilellas and F. Castro, *Mater. Sci. Eng. A*, 1996, **216**, 185.
- 5 A. Münster, *Z. Elektrochem.*, 1959, **63**, 807.
- 6 A. Münster and G. Schlamp, *Z. Phys. Chem.*, 1960, **25**, 116.
- 7 R. J. Irving and I. G. Worsley, *J. Less Common Met.*, 1968, **16**, 103.
- 8 R. Meyer and H. Pastor, *Bull. Soc. Fr. Céram. E*, 1969, **172**, 59.
- 9 J. Echeberria and F. Castro, *Mater. Sci. Technol.*, 1990, **6**, 457.
- 10 F. Castro, J. Echeberria and M. Fuentes, *J. Mater. Sci. Lett.*, 1992, **11**, 101.
- 11 J. Echeberria and F. Castro, in *Proceedings of First Euro-Ceramics V.3*, ed. G. With, R. A. Terpstra and R. Metselaar, Elsevier Applied Sciences, Essex, England, 1989, pp. 527–532.
- 12 P. Andrews and F. L. Riley, *J. Eur. Ceram. Soc.*, 1989, **5**, 245.
- 13 T. Moeller, *Inorganic Chemistry*, John Wiley & Sons, New York, 1965, p. 752.
- 14 M. G. Barandika, Ph.D. Thesis, Universidad de Navarra, 1995.
- 15 O. Knacke, O. Kubaschewski and H. Hesselman, *Thermochemical Properties of Inorganic Substances*, ed. O. Knacke, O. Kubaschewski and H. Hesselman, Springer-Verlag, Berlin, 1991.
- 16 *Phase Diagrams for Ceramists 1969 Supplement*, (2nd Printing), ed. M. K. Reser, The American Ceramic Society, OH, 1985, p. 6.
- 17 L. S. Sigl and K. A. Schwetz, *Powder Met. Int.*, 1991, **23**, 221.
- 18 L. S. Sigl and T. Jüngling, *J. Hard Mater.*, 1992, **3**, 391.

Paper 8/01121D; Received 9th February, 1998